Comparison of AIRS and IASI Radiances Using GOES Imagers as Transfer Radiometers toward Climate Data Records

LIKUN WANG,* XIANGQIAN WU,+ YAPING LI,# MITCH GOLDBERG,+ SEUNG-HEE SOHN,+,@ AND CHANGYONG CAO+

* *Perot Systems Government Services, Fairfax, Virginia*
+ *NOAA/NESDIS Center for Satellite Applications and Research, Camp Springs, Maryland*
# *I. M. Systems Group, Rockville, Maryland*
@ *Korea Meteorological Administration, Seoul, Korea*

(Manuscript received 10 March 2009, in final form 15 October 2009)

ABSTRACT

The Atmospheric Infrared Sounder (AIRS) and the Infrared Atmospheric Sounding Interferometer (IASI), together with the future Cross-track Infrared Sounder, will provide long-term hyperspectral measurements of the earth and its atmosphere at ~10 km spatial resolution. Quantifying the radiometric difference between AIRS and IASI is crucial for creating fundamental climate data records and establishing the space-based infrared calibration standard. Since AIRS and IASI have different local equator crossing times, a direct comparison of these two instruments over the tropical regions is not feasible. Using the Geostationary Operational Environmental Satellite (GOES) imagers as transfer radiometers, this study compares AIRS and IASI over warm scenes in the tropical regions for a time period of 16 months. The double differences between AIRS and IASI radiance biases relative to the *GOES-11* and *-12* imagers are used to quantify the radiance differences between AIRS and IASI within the GOES imager spectral channels. The results indicate that, at the 95% confidence level, the mean values of the IASI − AIRS brightness temperature differences for warm scenes are very small, that is, −0.0641 ± 0.0074 K, −0.0432 ± 0.0114 K, and −0.0095 ± 0.0151 K for the *GOES-11* 6.7-, 10.7-, and 12.0-μm channels, respectively, and −0.0490 ± 0.0100 K, −0.0419 ± 0.0224 K, and −0.0884 ± 0.0160 K for the *GOES-12* 6.5-, 10.7-, and 13.3-μm channels, respectively. The brightness temperature biases between AIRS and IASI within the GOES imager spectral range are less than 0.1 K although the AIRS measurements are slightly warmer than those of IASI.

1. Introduction

Measurements from hyperspectral infrared (IR) sounders on polar-orbiting satellites provide valuable information on atmospheric temperature and humidity profiles, greenhouse gases, clouds, and surface properties. Carried on the National Aeronautics and Space Administration's (NASA) Earth Observing System *Aqua* spacecraft with a 1330 LT ascending node and launched in May 2002, the Atmospheric Infrared Sounder (AIRS) is a grating-array imaging spectrometer that measures the thermal infrared spectrum with 2378 spectral channels covering the 3.75–4.59 μm (2181–2665 cm^{-1}), 6.20–8.22 μm (1217–1614 cm^{-1}), and 8.8–15.4 μm (650–1136 cm^{-1}) spectral regions with a nominal spectral resolution of $\nu/\Delta\nu = 1200$ (Chahine et al. 2006). The Infrared Atmospheric Sounding Interferometer (IASI) is the first operational interferometer in space measuring the 3.5–16.4-μm (610–2825 cm^{-1}) spectrum in 8461 spectral channels with a spectral resolution of 0.5 cm^{-1} and a spectral sampling interval of 0.25 cm^{-1}, successfully launched on board the Meteorological Operational Satellite Programme's *MetOp-A* in October 2006 with a 0930 descending node (Klaes et al. 2007). While primarily designed to improve numerical weather predications, the AIRS and IASI have the potential to provide a long-term record of accurately calibrated spectral radiances for climate monitoring and other climate-related studies because their high spectral resolutions offer inherent advantages for both radiometric and spectral calibrations (Goody and Haskins 1998). Therefore, quantifying the difference in their radiance measurements is crucial for generating fundamental climate data records. Moreover, since AIRS and IASI are being used as an on-orbit radiometric

Corresponding author address: Dr. Likun Wang, Rm. 810, 5200 Auth Rd., Camp Springs, MD 20746.
E-mail: likun.wang@noaa.gov

DOI: 10.1175/2009JAMC2218.1

© 2010 American Meteorological Society

reference to assess the calibration accuracy of other geostationary and polar-orbiting broad- and narrow-band instruments, understanding their radiometric biases and uncertainties is important for establishing the space-based IR calibration standard (Gunshor et al. 2009; Tobin et al. 2006; Wang et al. 2007, 2009; Wang and Cao 2008).

Two methods have been implemented to intercompare AIRS and IASI radiance measurements in previous studies: 1) a direct comparison at the orbital crossing point of satellites occurring at high latitudes—the so-called simultaneous nadir overpass (SNO) observations—either over relatively large wavelength intervals (Blumstein et al. 2007) or at the finest spectral scale (Tobin et al. 2008), and 2) using double differences between a pair of sensor radiance biases relative to a common transfer target (Aumann and Pagano 2008; Strow et al. 2008). Although the first approach can greatly reduce the uncertainties associated with the geometry and observational time differences of two sensors, the comparison is limited to high latitudes and thus cannot provide comprehensive bias structures because the bias can be climate regime dependent (Cao et al. 2009). The second approach, though limited to the stability of transfer targets (e.g., transfer radiometers and radiative transfer calculations), has the advantage of being able to extend the comparison beyond the polar regions to different climate regimes (e.g., warm tropical scenes) through an appropriate transfer target, which thus complements the SNO method.

Under the Global Space-Based Intercalibration System (GSICS) within the World Meteorological Organization's Space Programme, intercalibrations of geostationary imager infrared channels using AIRS and IASI are routinely performed at the Center for Satellite Applications and Research (STAR) of the National Environmental Satellite, Data, and Information Service (NESDIS) within the National Oceanic and Atmospheric Administration (NOAA) (Wu and Goldberg 2007). This GISCS strategy is illustrated as a three-way comparison in Fig. 1, which allows the intercalibration to be cross-validated through a different pair of instruments and thus facilitates the analysis for the root causes of biases. Specifically, the convolved AIRS and IASI radiances are compared with the geostationary imager radiance measurements using common spatial and temporal collocation criteria. Ideally, if IASI and AIRS are perfectly calibrated and consistent with each other, both should be able to detect the calibration biases of the geostationary imager equally. Consequently, the differences between the AIRS and IASI radiance biases relative to the reference geostationary imager should be close to 0. In other words, in addition to evaluating the calibration accuracy of geostationary imagers, the GSICS intercomparison results can indirectly compare AIRS and IASI via geostationary imagers with the double-difference method, in which the geostationary imagers are treated as transfer radiometers (indicated by the open arrow in Fig. 1). The *Geostationary Operational Environmental Satellite-11* and *-12* (*GOES-11* and *GOES-12*) imagers, positioned at (0°, 135°W) and (0°, 75°W), respectively, are chosen as transfer radiometers in this study. While both are five-channel imaging radiometers, the *GOES-12* imager has a new channel at 13.3 μm, replacing the 12.0-μm channel of *GOES-11*.

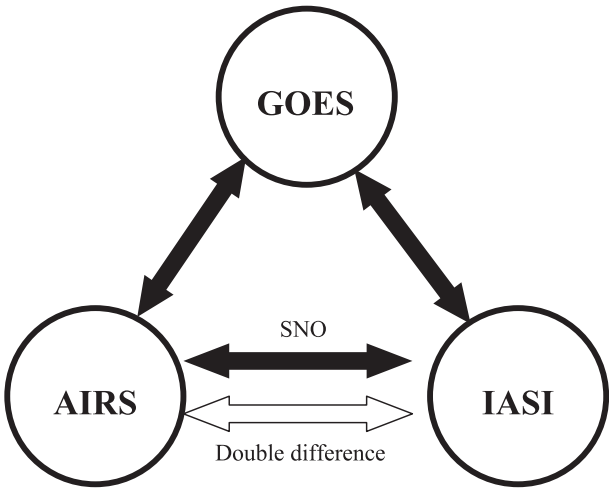

FIG. 1. Illustration of the GSICS intercalibration strategy.

This study serves two purposes. First, we demonstrate that a relatively stable geostationary instrument can be used as a transfer radiometer to intercompare polar-orbiting sensors. Second, this study extends the AIRS and IASI comparison to the tropical regions, complementing the existing SNO comparison, since AIRS and IASI have different local equator crossing times and a direct comparison of these two instruments is not feasible in the tropical regions.

This paper is organized as follows. Section 2 introduces the method used in this study. Section 3 presents the intercomparison results and section 4 concludes the paper.

2. Method

a. Instruments

For detailed descriptions of the AIRS, IASI, and GOES imager instruments, the reader is referred to other references (Blumstein et al. 2004; Chahine et al. 2006; Klaes et al. 2007; Schmit et al. 2001). Summarized in Table 1 are

TABLE 1. Instrument characteristics of AIRS, IASI, and the *GOES-11* and *-12* imagers.

	GOES-11 imager	*GOES-12* imager	*Aqua* AIRS	*MetOp-A* IASI
Local equator crossing time	—	—	1330	0930
Spectral coverage	One visible channel (0.65 μm) One shortwave IR channel (3.9 μm) Three longwave IR channels (6.7, 10.7, and 12.0 μm)	One visible channel (0.65 μm) One shortwave IR channel (3.9 μm) Three longwave IR channels (6.5, 10.7, and 13.3 μm)	2378 channels (3.7–15.4 μm)	8461 channels (3.6–15.5 μm)
Instantaneous FOV at nadir	Visible channel 1.0 km IR channels 8 km for 6.7-μm channel; 4.0 km for other three channels	Visible channel 1.0 km IR channels 8 km for 13.3-μm channel; 4.0 km for other three channels	13.5 km	12.0 km
Earth scan angle	21°N/S × 23°E/W	21°N/S × 23°E/W	±49.5° from nadir	±48.3° from nadir
Scan samplings	5460 samples for IR channel; 21 840 samples for visible channel	5460 samples for IR channel; 21 840 samples for visible channel.	90 footprints	30 footprints (each containing four pixels)
Calibration	Two-point radiometric calibration	Two-point radiometric calibration	Two-point radiometric calibration; spectral calibration using atmosphere spectral features	Two-point radiometric calibration; spectral calibration using atmosphere spectral features for offline diagnosis

the instrument characteristics. The simulated AIRS and IASI spectra, as well as the GOES imagers spectral response functions (SRFs), are given in Fig. 2.

AIRS is a grating IR sounder that disperses the radiation from the earth scene onto 17 linear arrays of Hg–Cd–Te detectors on a focal plane with 2378 IR channels. AIRS views the ground through a cross-track rotary scan mirror that provides ±49.5° ground coverage every 2.67-s scan cycle. A total of 90 ground footprints is observed for each scan with each footprint containing all 2378 spectral samples. The AIRS IR spatial resolution is 13.5 km from the nominal altitude of 705.3 km with a 1330 ascending node. The on-orbit calibration of AIRS involves radiometric and spectral calibrations. Routine IR radiometric calibration data are taken while the scan mirror rotates from −49.5° (relative to nadir) through 180° (antinadir position) to +49.5°. These data consist of four independent views of cold space and one view of the onboard blackbody, and are used to derive the radiometric gain (slope) and offset (intercept). The nonlinearity correction is performed by using the prelaunch calibration data. The selected atmospheric spectral features with simulated upwelling radiances are compared with AIRS to diagnose possible shifts of each feature relative to the nominal grating model. The AIRS version 5 data are used in this study.

IASI on *MetOp-A* is a Michelson interferometer that measures infrared radiation emitted from the earth in the infrared spectra between wavelengths of 3.6 and 15.5 μm (Blumstein et al. 2004). IASI is in a sun-synchronous polar orbit at 819 km with a 0930 equator cross in a descending node. The IASI observations are obtained by a step scanning mirror covering ±47.85° range in 30 steps in every 8.0-s scan cycle, with 3.3° for each step (normal mode). At each step, the field of regard (FOR) includes 2 × 2 1.25° fields of view (FOVs) with a pixel resolution of 12 km at nadir, each positioned in the cross- and along-track directions located at ±0.825°. The measured interferograms are processed by an onboard digital processing subsystem in order to reduce the data transmission rate, which performs the inverse Fourier transform, the radiometric calibration (based on the measurements of cold and warm reference targets, i.e., deep space and an onboard blackbody), and nonlinearity corrections. The ground processing includes radiometric postcalibration, spectral calibration, and apodization, which produces resampled, apodized, and calibrated spectra with 8461 spectral samples, that is, IASI level-1C radiance products.

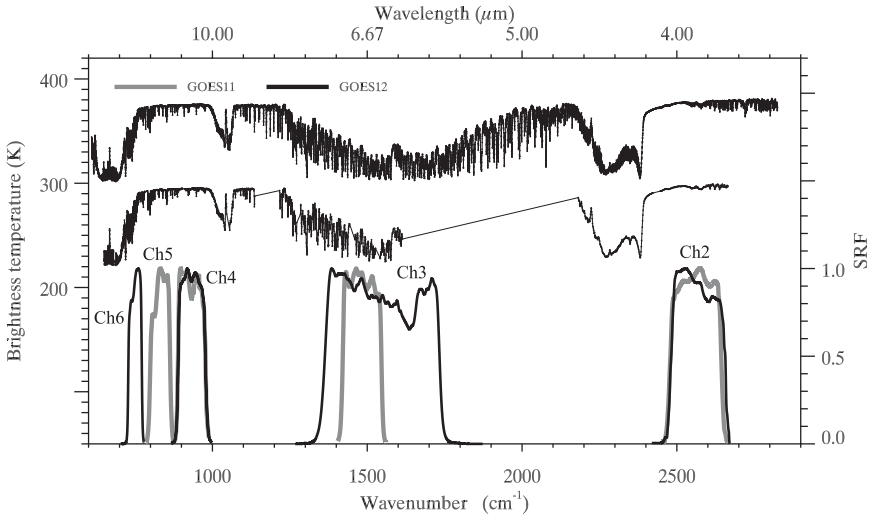

FIG. 2. IASI (top black line) and AIRS (middle black line) BT spectra calculated from the Community Radiative Transfer Model (CRTM) overlaid with the spectral response functions of the *GOES-11* and *-12* imagers. Note that the IASI BT spectrum is displaced by 80 K in order to separate it from the AIRS spectrum for comparison.

The *GOES-11* and *GOES-12* imagers are five-channel imaging radiometers, including one visible channel (0.65 μm), one shortwave IR channel (3.9 μm), and three longwave IR channels (6.7, 10.7, and 12.0 μm for *GOES-11*; 6.5, 10.7, and 13.3 μm for *GOES-12*). Compared to the *GOES-11* imager, the *GOES-12* imager has a spectral channel centered at 13.3 μm, replacing the previous 12.0-μm channel. The *GOES-12* imager also includes a spectrally modified 6.5-μm channel with an improved spatial resolution from 8 to 4 km at the subsatellite point. As a trade-off, the *GOES-12* 13.3-μm channel's spatial resolution is approximately 8 km in the north–south direction, the same as that of the 6.7-μm channel of *GOES-11* (Table 1). In other words, the detectors used for the *GOES-12* 13.3-μm and *GOES-11* 10.7-μm channels have an instantaneous geometric field of view (IGFOV) of 224 μrad, resulting in a subsatellite pixel of 8 km on a side, while the detectors for the other three IR channels have an IGFOV of 112 μrad, corresponding to a square 4-km pixel at the subsatellite point. Because of the combination of scan rate (20° s^{-1}) and detector sample rate (5460 samples per second for the IR channels and 21 840 samples per second for the visible channel), each sample step corresponds to an angle of 16 μrad for the visible channel and 64 μrad for the IR channels along a scan line. In other words, the GOES imager oversamples the infrared IGFOVs of 4 and 8 km along a scan line by factors of 1.75 and 3.5, respectively. During the instrument's operation, the infrared channels are frequently calibrated based on space-view and onboard blackbody view observations, providing an absolute calibration accuracy of better than 1.0 K with 0.3-K relative precision (Boeing 2006).

b. Method

Three major steps are involved for the intercomparison of the AIRS and IASI radiances using geostationary imagers as transfer radiometers, including 1) spectral convolution, 2) spatial and temporal collocation for AIRS/IASI and the GOES imagers' observations, and 3) statistical calculations. These three steps are described in this section.

1) SPECTRAL CONVOLUTION

The objective of spectral convolution is to integrate the hyperspectral radiance spectrum to match the broadband GOES imager SRF and make it comparable with the GOES imager observations. Given the hyperspectral radiance $R(\nu)$ at each wavenumber ν, it can be convolved with the GOES imager SRF $S(\nu)$ to generate the IASI- or AIRS-simulated GOES imager infrared channel radiance L as

$$L = \frac{\int_{\nu_1}^{\nu_2} R(\nu)S(\nu)\,d\nu}{\int_{\nu_1}^{\nu_2} S(\nu)\,d\nu}, \tag{1}$$

where ν_1 and ν_2 are the spectral bandpass limits. The GOES imager SRFs can be obtained online (http://cimss.ssec.wisc.edu/goes/calibration/).

A major issue in spectral convolution for AIRS is estimating the missing spectral radiance values either by design or due to dead or unstable detectors. A common practice is to replace these radiance values with simulated atmospheric spectra, the so-called AIRS gap-filling technique (Gunshor et al. 2009; Tobin. et al. 2006). The GSICS intercalibration algorithm uses the method proposed by Tahara and Kato (2008). In their method, the atmospheric spectra for eight different atmospheric profiles (including both cloudy and clear-sky conditions) are simulated by the Line-by-Line Radiative Transfer Model (LBLRTM). The relationship between the simulated and observed radiances for the AIRS good channels is then established by solving a linear least squares problem. The radiance values of missing AIRS channels are then predicated based on this relationship. The accuracy of the gap-filling method has been reviewed by Tahara and Kato (2008). It shows that the gap-filling method has minimal effects (smaller than 0.001 K) on the channels where the AIRS individual channels are missing due to the dead or unstable detectors, but yields significant improvements in the spectral regions that AIRS does not fully cover. It is known that only the *GOES-12* water vapor channel suffers from the uncertainties due to the AIRS spectral gap filling (see Fig. 2).

2) Spatial and temporal collocation

In the second step, the AIRS and IASI measurements are collocated to the GOES observations in space, time, and view geometry. The strategy is to find the geostationary satellite measurements that fall inside the pixels of the polar-orbiting satellites by minimizing the observational time and view geometry differences. First, the time difference between IASI–AIRS and geostationary observations is constrained to less than 300 s in this study. The sensitivity test performed in this study—as well as those done by others (Gunshor et al. 2009; Wang et al. 2009)—indicates that, given a relatively uniform scene, tightening the time collocation criterion reduces both the standard deviation of the IASI–AIRS − GOES brightness temperature (BT) differences and the number of collocations, but does not significantly impact the mean value of the BT differences. The 300-s time window is chosen as a compromise to keep a sufficient number of samples and also reduce the effects caused by instrument observational time difference.

Two identical satellite instruments sensing the same target at the same time should obtain the same measurements only if they have identical lines of sight, that is, if their zenith angles from the target are the same and their relative azimuth angles equal zero. Within the infrared spectrum, where AIRS and IASI cover, a similar view zenith angle means a similar geometric pathlength, which implies a similar optical pathlength. Since the secant of the zenith angle is approximately proportional to the optical pathlength, the relative difference between the secant of the two zenith angles from geostationary and polar-orbiting satellites can be used to limit the optical path difference, which is expressed as |cos(geo_zen)/cos (leo_zen)-1|, where geo_zen and leo_zen represent the view zenith angles of the geostationary and polar-orbiting satellites, respectively. The criterion of this parameter is set to 0.01 or less in this study. This requirement allows 8.07° of zenith angle difference at nadir and 0.327° at 60° zenith angle, respectively.

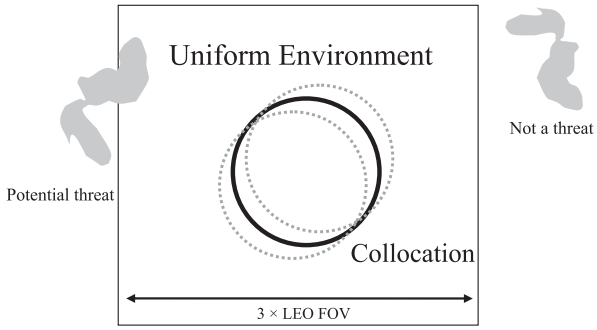

FIG. 3. Illustration of a uniform environment. The center circle in the solid line is a collocation target. The two dashed circles are possible locations of actual geostationary and polar-orbiting instrument FOVs, due to navigation uncertainty and collocation limitation. The large square in the solid line is the collocation environment. The two gray objects are examples of nonuniform features, where the one on the left is a potential threat to collocation whereas the one on the right is not.

A minimal relative azimuth angle is required for visible and near-infrared channels due to scene bidirectional reflectance characteristics. For infrared window channels and absorptive channels, if the scene and atmosphere are highly inhomogeneous (e.g., when clouds exist), longwave emission may be anisotropic. To reduce the azimuth angle effects, the comparison is limited to uniform scenes, and also excludes the shortwave IR channels.

A spatially uniform environment surrounding the collocated measurements is desirable to compensate for minor violations of collocation and coincidental criteria as well as to reduce the uncertainties caused by azimuth angle differences and navigation errors. In our implementation, the collocation environment is defined as 3 times the FOVs of the polar-orbiting instruments, as shown in Fig. 3. The environment uniformity is measured by the standard deviation of radiance relative to the mean radiance, expressed as

$$\sigma_{\mathrm{env}}/\overline{L}_{\mathrm{env}} \leq 0.05, \tag{2}$$

where σ_{env} and $\overline{L}_{\mathrm{env}}$ are the standard deviation and mean of the environment radiance, respectively. In addition,

for each collocated AIRS/IASI–GOES FOV, the ratio of the standard deviation and the mean of the GOES radiances is also required to be less than 0.01:

$$\sigma_{\mathrm{fov}}/\overline{L}_{\mathrm{fov}} \leq 0.01, \tag{3}$$

where σ_{fov} and $\overline{L}_{\mathrm{fov}}$ are the standard deviation and mean of the GOES radiances within the collocated AIRS/IASI–GOES FOV, respectively.

3) STATISTICAL CALCULATION

For each collocated AIRS/IASI–GOES FOV, the brightness temperatures (BTs) are computed from the IASI–AIRS-convolved radiance and the mean of GOES radiances, respectively. The BT differences between AIRS–IASI and the GOES imager are derived. Given hundreds of collocations for each day, the mean BT difference is calculated, which represents the GOES observation bias relative to AIRS and IASI. The double differences between the AIRS and IASI radiances relative to the GOES imagers in terms of BTs is defined as

$$\Delta T = \langle \mathrm{BT}_{\mathrm{GEOS}} - \mathrm{BT}_{\mathrm{AIRS}} \rangle_{\mathrm{mean}} - \langle \mathrm{BT}_{\mathrm{GEOS}} - \mathrm{BT}_{\mathrm{IASI}} \rangle_{\mathrm{mean}}, \tag{4}$$

where $\mathrm{BT}_{\mathrm{AIRS}}$, $\mathrm{BT}_{\mathrm{IASI}}$, and $\mathrm{BT}_{\mathrm{GOES}}$ are the BT values from AIRS, IASI, and the GOES imagers, respectively, for one collocation pair. Note that the subscript of "mean" indicates an average over a day. To cancel out the impacts of the transfer radiometers, the transfer radiometer itself must be stable during the AIRS/IASI–GOES collocation. In other words, since AIRS and IASI pass over the geostationary satellite nadirs two times each day at a fixed local time (i.e., 0130–1330 and 0930–2130), any diurnal calibration difference of the GOES imagers can introduce systematic errors into the final results. It is well known that the computed calibration slopes for the GOES imager infrared channels exhibit anomalous dips during the approximate 6 h centered on satellite midnight, which is believed to be interference by stray radiation from solar-heated structural components that reaches the imager detectors during the blackbody look (Johnson and Weinreb 1996). While corrections have been made for the GOES radiance data, our analysis still indicates that this calibration problem exists for the GOES midnight observations as compared with the observations from other time periods. Thus, this study is limited to daytime data only.

c. *Uncertainty analysis*

In general, two types of errors can be introduced into the bias statistics: 1) those introduced by random processes and 2) systematic biases. The purpose of this study is to identify the systematic radiometric difference between AIRS and IASI within the spectral channels of the GOES imagers. To detect the systematic errors related to the AIRS and IASI measurements, it is expected that the method is able to avoid possible systematic errors from other sources and minimize random errors through the collocation and convolution. The remainder of the random errors can be further reduced to a negligible level by averaging enough samples.

The possible sources of random errors are 1) the instrument radiometric noise levels of AIRS, IASI, and the GOES imagers; 2) view zenith angle and azimuth angle differences; 3) collocation uncertainties due to each instrument's navigation errors; 4) the observational time difference; 5) other errors related to scene nonuniformity and instrument footprint size difference; and 6) the spectral gap-filling errors (only for the *GOES-12* water vapor channel). The instrument noise of AIRS, IASI, and the GOES imagers has a Gaussian distribution. Spectral convolution should filter out the AIRS and IASI instrument noise. The average of the daily samples further reduces the noise of the GOES imagers as well as other IASI and AIRS instrument noise. The bias related to the spectral gap filling is only a concern for the *GOES-12* water vapor channel (6.5 μm), due to its relatively large spectral gap. Recall that the predicated relationship used to calculate the AIRS spectral-gap radiances is generated by solving a least squares problem. A sensitivity test based on different atmospheric profiles indicates that errors caused by the spectral gap filling are dependent on the collocation environment and thus are random rather than systematic. Given hundreds of collocated samples each day in different collocation environment, the average will minimize this error. The collocation uncertainties due to each instrument's navigation errors and the differences in instrument footprint size are minimized with the help of collocation criteria and the uniformity of the collocated FOV and environment, as well as taking the average. Figure 4 gives the GOES – AIRS BT difference distribution with respect to the observational time and zenith angle differences, the relative azimuth angle between AIRS and GOES, as well as the collocated FOV scene uniformity for *GOES-12* channel 6 data taken during the daytime of 3 July 2007. Figure 4 clearly shows that the BT differences are randomly distributed along their mean value with the zenith angle, azimuth angle, and observational time differences as well as scene uniformity. In other words, the mean BT difference does not depend on these parameters.

The factors that may cause the systematic biases but are not related to AIRS and IASI are the calibration

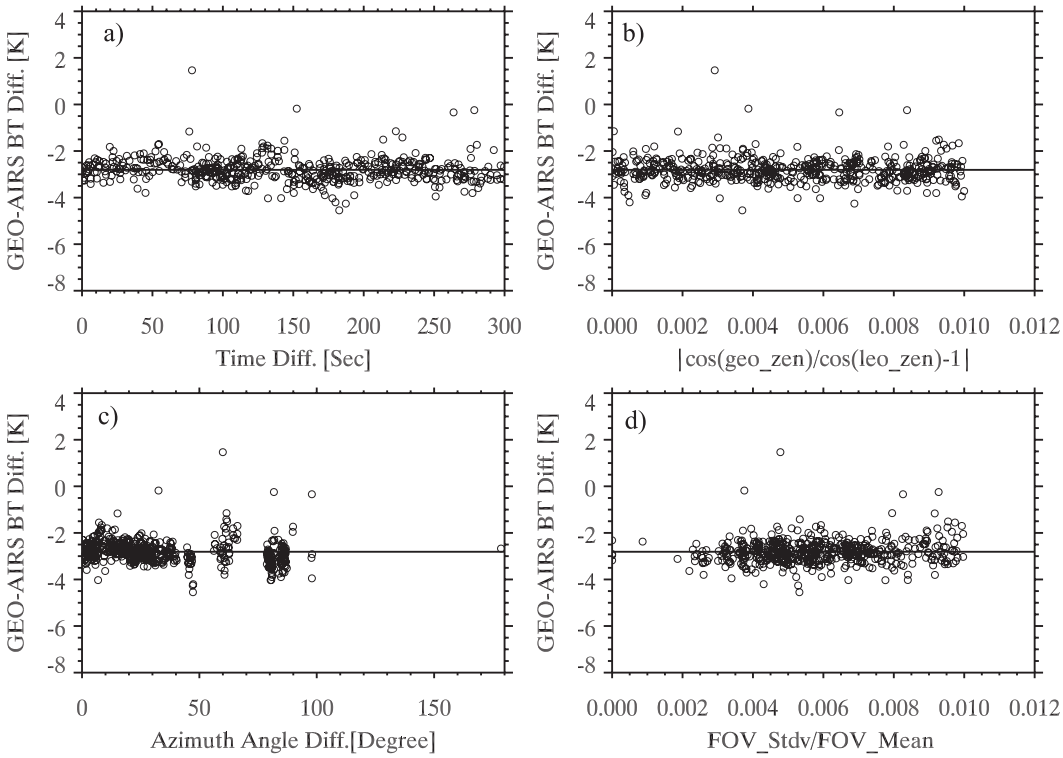

FIG. 4. The GOES – AIRS BT difference distribution with (a) the observational time and (b) the zenith angle differences, (c) the relative azimuth angle between AIRS and GOES, as well as (d) the collocated FOV scene uniformity for *GOES-12* channel 6 on 3 Jul 2007 (only for daytime collocation). The solid line indicates the mean BT difference of −2.83 K.

bias of each GOES imager, for example, diurnal and seasonal calibration bias, instrument sudden-change-induced bias, and SRF-uncertainty-caused bias. As we discussed above, the day–night calibration bias is avoided by choosing daytime observations only. The GOES diurnal calibration variation during the daytime has been examined by binning the collocation data according to the observation time. We did not observe any calibration variation pattern for a 4-h time window during the daytime period. In other words, given a 4-h time window from 0930 to 1330 (local time at satellite subpoints), the calibration of the GOES imagers is stable so that no systematic calibration bias is introduced. Through a double-difference method, other calibration biases of the GOES imagers are expected to be canceled out. Therefore, we believe that the final results from the double differences are mainly related to the systematic bias due to the AIRS–IASI measurement difference.

3. Results and discussion

The data used in this study extend from 1 June 2007 to 30 September 2008 and cover 16 months until this paper was finalized. Some days are missing because of the instrument operational anomalies. Note that the double differences are only calculated for the days when both IASI–GOES and AIRS–GOES collocations existed. The time series of the GOES–AIRS and GOES–IASI daily mean BT differences, as well as their double differences, are given in Figs. 5 and 6 for the *GOES-12* and *-11* imagers, respectively.

a. Intercalibration capabilities

As discussed above, the AIRS and IASI hyperspectral radiances are often used to assess the calibration accuracy of geostationary imagers (Gunshor et al. 2009; Wang et al. 2009). Here, we believe that these intercalibration results can also be used to quantify the AIRS and IASI radiance difference. Since this comparison involves four sensors (i.e., AIRS, IASI, and the *GOES-11* and *-12* imagers), the intercalibration results can be cross validated through different pairs of instruments to facilitate the root cause analysis for the bias. Examples are presented below to demonstrate these capabilities.

The first example begins with *GOES-12* channel 6 (13.3 μm), shown in Fig. 5c. The time series plot of the GOES – AIRS BT difference (indicated by the red dots) depicts a sudden change around 2 July 2007 (jump from

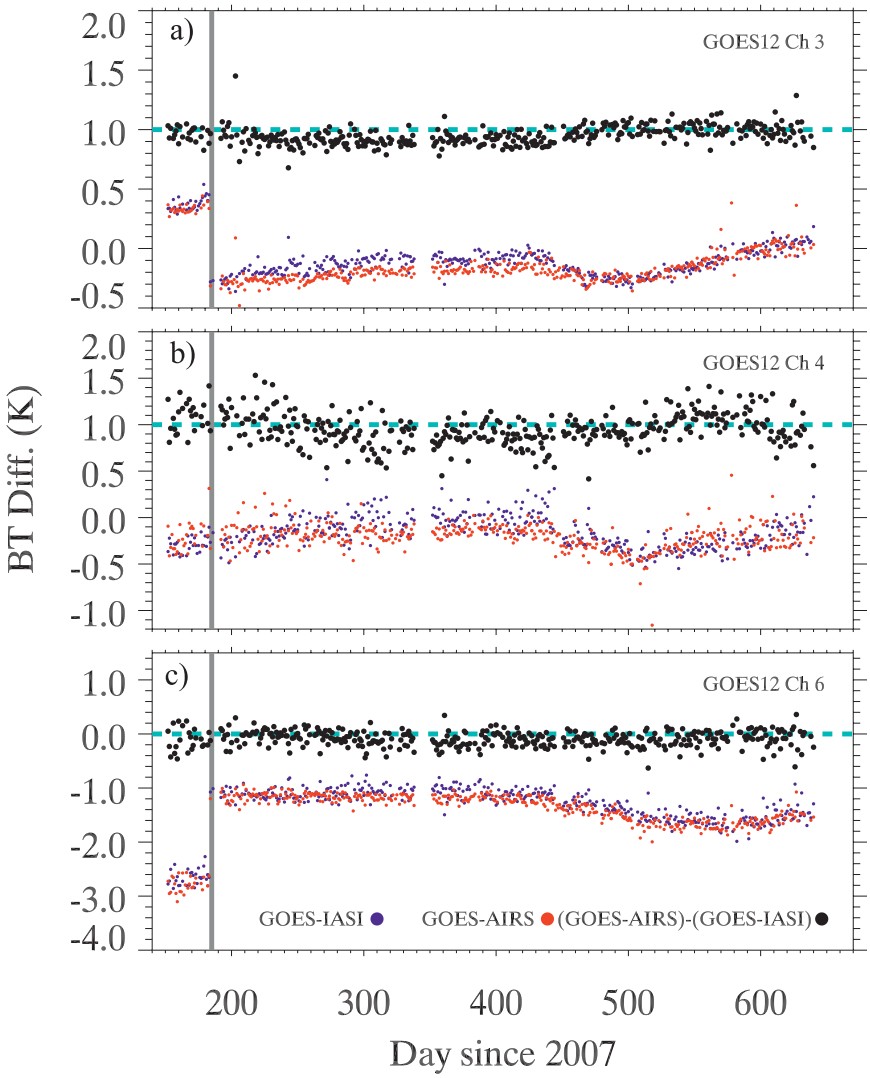

FIG. 5. Time series of the GOES – AIRS and GOES – IASI daily mean BT difference as well as their double differences for the (top to bottom) *GOES-12* three longwave IR channels. The dashed horizontal lines indicate the 0 value. Note that the double difference has been displaced by 1.0 K for channels 3 and 4. The data gap around December 2007 is due to *GOES-12*'s operational failure. The solid vertical line indicates 4 Jul 2007, when the *GOES-12* decontamination was performed.

−2.5 to −1.0 K). After that, the BT difference remained relatively constant (∼−1.0 K) till it gradually decreased after April 2008. However, the comparison of these two sensors cannot determine which instrument, either AIRS or the *GOES-12* imager, caused the cold bias. In other words, additional information is needed to identify the root cause of the bias. The GOES and IASI intercalibration (represented by the blue dots) time series indicates the same features, which confirms that this cold bias is caused by the *GOES-12* imager. Further investigation indicates that the *GOES-12* imager experienced a decontamination procedure from 2 to 4 July 2007, where certain internal components were warmed up in an attempt to drive off contaminants (mainly water ice). This instrument change apparently impacted the *GOES-12* calibration accuracy, which was confirmed by both IASI and AIRS. It is of particular interests that the double-difference time series (shown as the black dots in Figs. 5c) removed the sudden change and the later gradual decrease of the bias, and remained constant during the entire time period. This suggests the excellent calibration of IASI and AIRS because both can track the GOES imager calibration bias well. The same feature can also be found for *GOES-12* channel 3 (6.5 μm) (Fig. 5a).

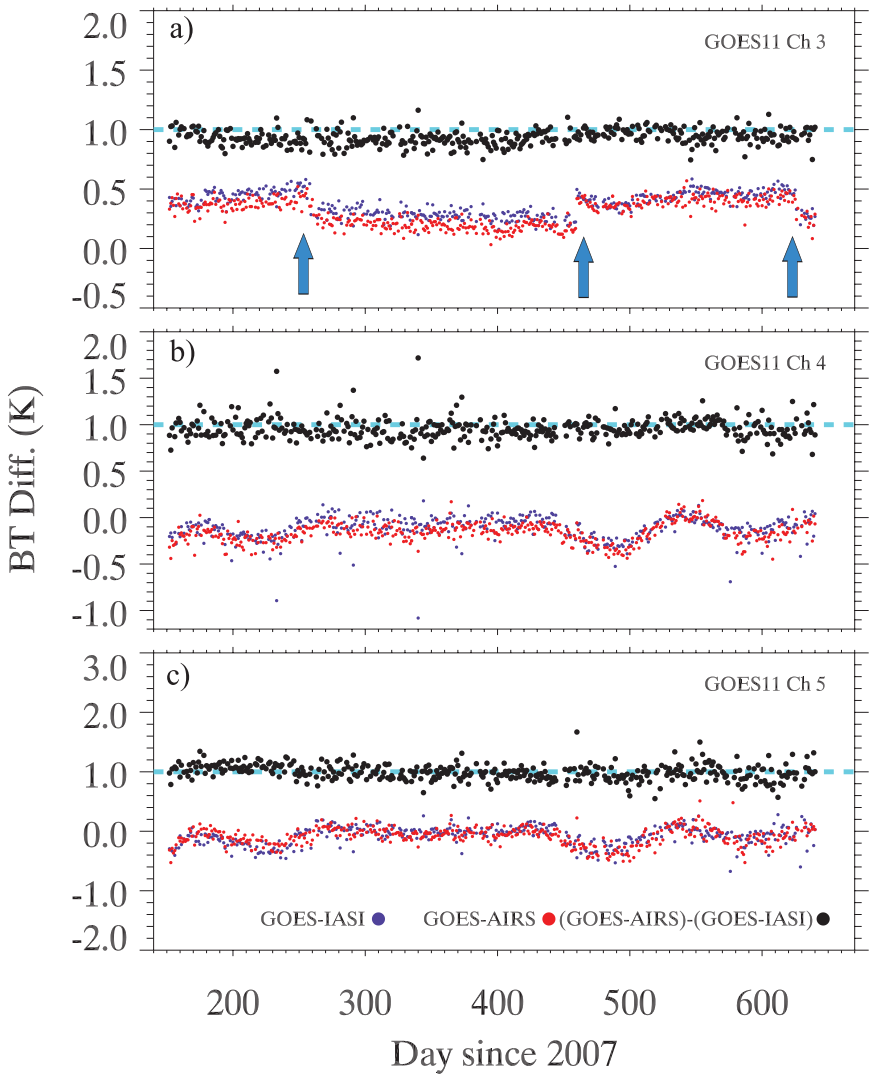

FIG. 6. As in Fig. 5, but for the *GOES-11* imager. Note that the double difference has been displaced by 1.0 K. The blue arrows designate the time when the *GOES-11* detector patch temperature was changed.

Figure 6a, for *GOES-11* channel 3 (6.7 μm), serves as another example to show this capability. There are pronounced fluctuations along the GOES–AIRS and GOES–IASI BT time series (represented by the red and blue dots), indicating that they are caused by the *GOES-11* imager change. We found that the detector patch temperature of *GOES-11* was raised from 91 to 99 K in the summertime and lowered from 99 to 91 K in the wintertime, as indicated by the blue arrows in Fig. 6a. Since the patch is on the north-facing side of the satellite, it runs warmer in the summertime. The float patch temperature often causes a variable instrument noise. As a trade-off, the patch temperature is raised in summer in order to keep the stable (constant) patch temperature. It is expected that the GOES calibration accuracy should not be impacted by this patch temperature change. However, both IASI and AIRS successfully track the calibration accuracy change caused by the patch temperature change. More interestingly, the IASI and AIRS double differences were not impacted and remained consistent before and after the *GOES-11* patch temperature change. The above discussion further demonstrates that systematic errors related to the calibration accuracy of the transfer radiometer calibration are canceled out through the double-difference calculations. These results have been encouraging enough to merit further investigation of the IASI and AIRS radiance difference through the double differences.

The 10.7-μm channels of the *GOES-12* and *-11* imagers are presented as a final example, given in Figs. 5b

TABLE 2. Double-difference statistics between the AIRS and IASI radiances relative to the *GOES-11* and *-12* imagers in terms of BT.

	GOES-11			*GOES-12*		
	Channel 3	Channel 4	Channel 5	Channel 3	Channel 4	Channel 6
Central wavelength (μm)	6.7	10.7	12.0	6.5	10.7	13.3
Sample no.	405	402	400	388	384	388
Lag-1 autocoef	0.157	0.066	0.140	0.260	0.253	0.084
Mean (K)	−0.0641	−0.0432	−0.0095	−0.0490	−0.0419	−0.0884
Std dev (K)	0.0649	0.1092	0.1341	0.0770	0.1733	0.1478
95% confidence interval (K)	0.0063	0.0107	0.0131	0.0077	0.0173	0.0147
Adjusted 95% confidence interval (K)	0.0074	0.0114	0.0151	0.0100	0.0224	0.0160
Trend (K yr^{-1})	0.0286	0.0080	−0.0829	0.0730	−0.0009	−0.0175
Uncertainty (K yr^{-1})	0.0083	0.0141	0.0170	0.0096	0.0233	0.0197
Adjusted uncertainty (K yr^{-1})	0.0097	0.0151	0.0195	0.0125	0.0302	0.0214

and 6b. As indicated by Fig. 2, these two channels have the same spectral coverage. The double differences for these two channels, which are used to quantify the AIRS–IASI difference, should give similar results within their uncertainties regardless of which transfer radiometer is chosen. To make it clear, we summarize the statistics of the double differences (shown in Figs. 5 and 6) in Table 2. The double-difference results for *GOES-11* and *-12* channel 4 (the mean and 95% confidence level) are consistent to each other within the uncertainties. Note that the standard deviation of *GOES-12* is larger than that of *GOES-11* because the collocations for *GOES-12* occurred more over land and hence contained more inhomogeneous scenes than *GOES-11*. The above example confirms the effectiveness of the double-difference method, which is not sensitive to the transfer radiometer.

In summary, the above discussion demonstrates that the variations in the GOES – AIRS and GOES – IASI BT differences can well track the relative consistency between AIRS and IASI in spite of sudden changes or gradual variations of the GOES imager calibration accuracy. In the discussion that follows, we thus focus on the AIRS and IASI radiance differences revealed by the double differences.

b. IASI and AIRS difference

The statistics of the double differences, which are used to characterize the IASI and AIRS radiance differences in terms of BT within the GOES imager spectral channels, are summarized in Table 2. Histograms of the double differences, shown as the gray bars in Fig. 7, are overlaid with fitted Gaussian distributions. The reduced chi-squared statistic $\chi_\upsilon^2(=\chi^2/\upsilon)$ where χ^2 is the chi-squared statistics and υ the degrees of freedom) can be used to describe the goodness of fit of the computed values to the data. As noted by Bevington and Robinson (2003), ideally, a value of $\chi_\upsilon^2 = 1$ implies the best fit of the given data. Values of χ_υ^2 much larger than 1 result from large deviations from the assumed distribution and may indicate poor measurements, incorrect assignment of uncertainties, or an incorrect choice of the probability function. The calculated χ_υ^2 values range from 1.53 to 2.83 (given in Fig. 7), indicating that the distributions of the double differences approximate a normal or Gaussian distribution in practice. Therefore, it is possible to use the Student's *t* test to estimate the 95% confidence interval of those differences using

$$\sigma_{95\%} = \pm t_{0.025}\frac{\sigma}{\sqrt{N}}, \tag{5}$$

where $t_{0.025}$ is the Student's *t* test's critical point for a large sample number and is equal to 1.96, σ is the standard deviation of the double differences, and N is the sample number. The null hypothesis is that the differences in the mean values of both the GOES – AIRS and GOES – IASI BT differences are zero (or that the mean values are equal). The formula given above for the error estimation is, however, only correct if the individual data points are unrelated, or statistically independent. As described in Santer et al. (2000), a common and relatively simple method can be used to correct the autocorrelation effects by determining the effective sample size $N_{\rm eff}$:

$$N_{\rm eff} = \frac{N(1-R_1)}{(1+R_1)}, \tag{6}$$

where R_1 is the lag-1 autocorrelation coefficient and N is the sample number from the data. The adjusted 95% confidence level based on the above method is given in Table 2.

At the 95% confidence level, the mean values of the IASI–AIRS brightness temperature differences are −0.0641 ± 0.0074 K, −0.0432 ± 0.0114 K, and −0.0095 ± 0.0151 K for the *GOES-11* 6.7-, 10.7-, and 12.0-μm channels, and −0.0490 ± 0.0100 K, −0.0419 ± 0.0224 K, and −0.0884 ± 0.0160 K for the *GOES-12* 6.5-, 10.7-, and 13.3-μm channels. Note that the results from the

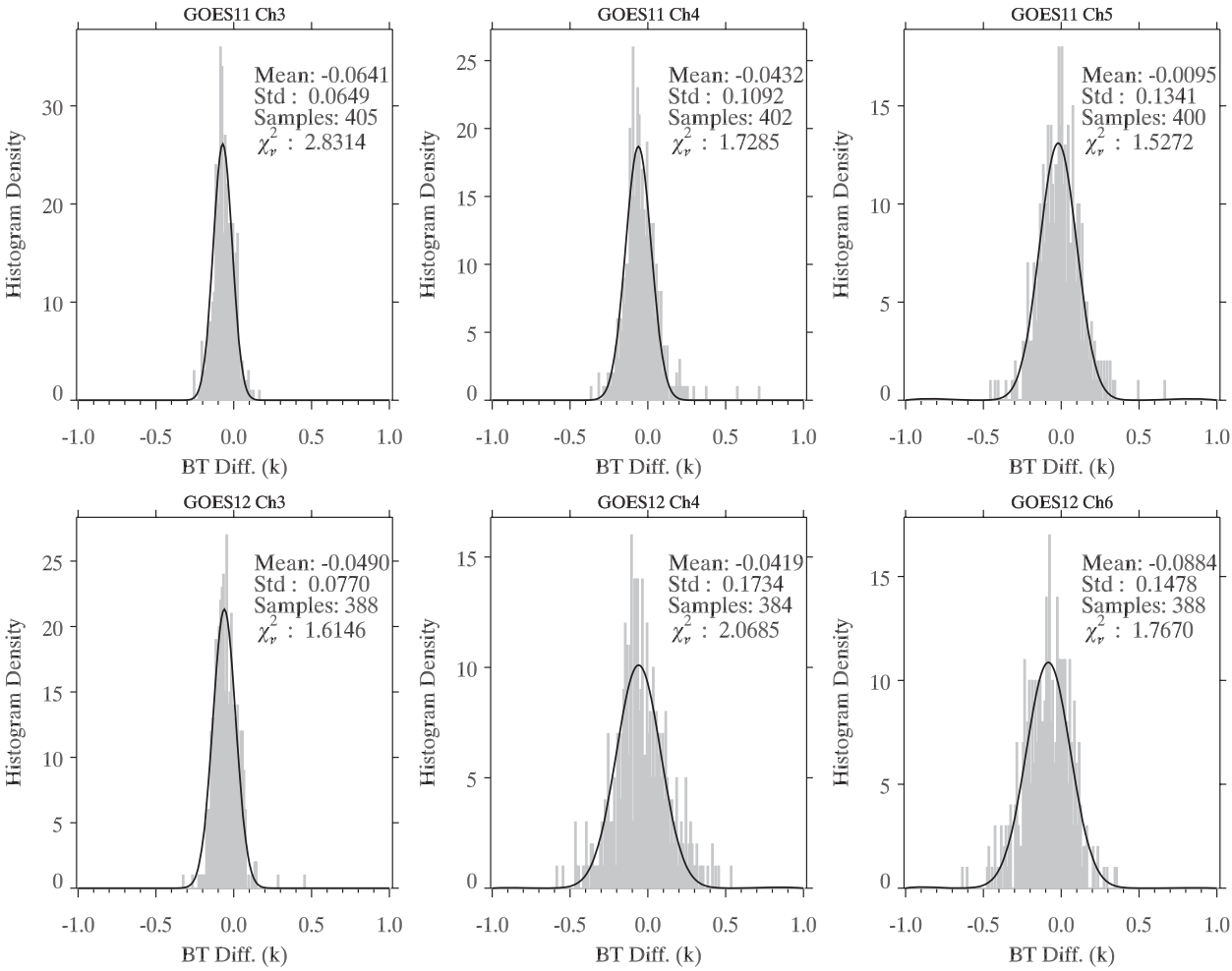

FIG. 7. Histograms of the double differences between GOES – AIRS and GOES – IASI (the gray bars), overlaid with computed Gaussian distributions (the black curves). The title of each panel denotes the instrument name and channel number. The values of the mean, standard deviation, sample number, and reduced chi-square parameter are listed. Note that the bin size is 0.01 K.

GOES-12 6.5-μm channel should be viewed with caution due to the spectral gap filling. AIRS and IASI have the best agreement within *GOES-11* 12.0-μm channel (channel 5; i.e., -0.0095 ± 0.0151 K). For the CO_2 absorption channel (*GOES-12* channel 6 at 13.3 μm), AIRS and IASI have a relatively larger cold bias (-0.0884 ± 0.0160 K) than do the other channels. Generally speaking, the radiance differences between AIRS and IASI within the GOES imager channels is less than 0.1 K while AIRS is slightly warmer than IASI.

Note that the largest uncertainty value is found for the *GOES-12* 10.7-μm channel while the two water vapor channels have the smallest values, which is due to scene inhomogeneity as discussed above. This suggests that the preciseness of the double-difference method is impacted by scene uniformity, which is a key factor in controlling the uncertainties caused by the minor violations of the collocation and concurrence, as well as the view geometry difference.

To characterize the IASI – AIRS BT difference variation with time, we also calculate the linear trend of the double-difference time series, as well as one sigma uncertainty with autocorrelation correction, given in Table 2. Except for the two water vapor channels, there is no statistically significant trend because the uncertainty is larger than or comparable to the trend value. More interestingly, small seasonal variations can be found from the double-difference time series of *GOES-12* channels 3 and 4, as well as *GOES-11* channel 3. However, the statistical period in this study is too short, so it cannot determine statistically significant trends for the IASI and AIRS BT differences, as well as the seasonal variations. We will extend the time series and revisit this issue in the future.

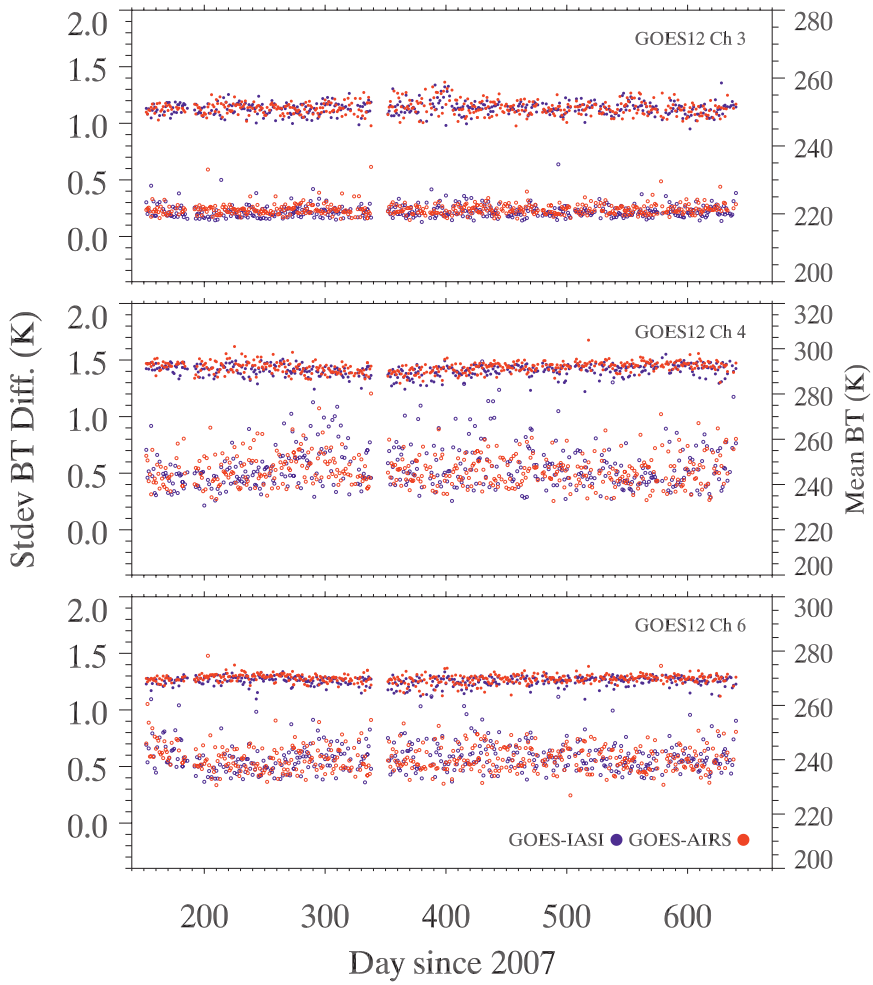

FIG. 8. Time series of the mean GOES BT (solid circles) and standard deviation of the BT difference (open circles) for the AIRS–IASI and *GOES-12* collocations.

Figures 8 and 9 present the time series of the standard deviation of the BT difference and mean GOES BT for the GOES–AIRS and GOES–IASI collocations for *GOES-12* and *-11*, which provide information about random errors and scene temperatures. The standard deviations of both GOES–AIRS and GOES–IASI BT differences are stable with time, indicating that the random errors do not vary much during the time period. The time series of the GOES mean BT show that the AIRS and IASI comparison is performed for relatively warm scenes, that is, ~290 K for the window channels, ~220 K for the water vapor channels, and ~270 K for the CO_2 channel. These values are also relatively constant with time in this study.

It is not possible, from this study, to address the absolute calibration accuracy for both the AIRS and IASI instruments by means of intersatellite comparison results. However, the small relative difference between AIRS and IASI disclosed from this study provides useful information for climate-related studies using the IASI and AIRS data.

c. *Discussion*

It is not a novel approach to indirectly compare two sensors through a third transfer target using the double-difference technique. For example, Wu et al. (2008) conducted an intercomparison of the two Moderate Resolution Imaging Spectroradiometers (MODISs) on board *Terra* and *Aqua* using the Advanced Very High Resolution Radiometer (AVHRR) on board the NOAA-KLM series of satellites as a transfer radiometer. Strow et al. (2008) employed radiative transfer calculations using global model output to indirectly compare AIRS and IASI at the finest scale. Aumann and Pagano (2008) chose the Real Time Global Sea Surface Temperature (RTGSST) from the National Centers for Environmental Prediction in the tropical ocean as a transfer target,

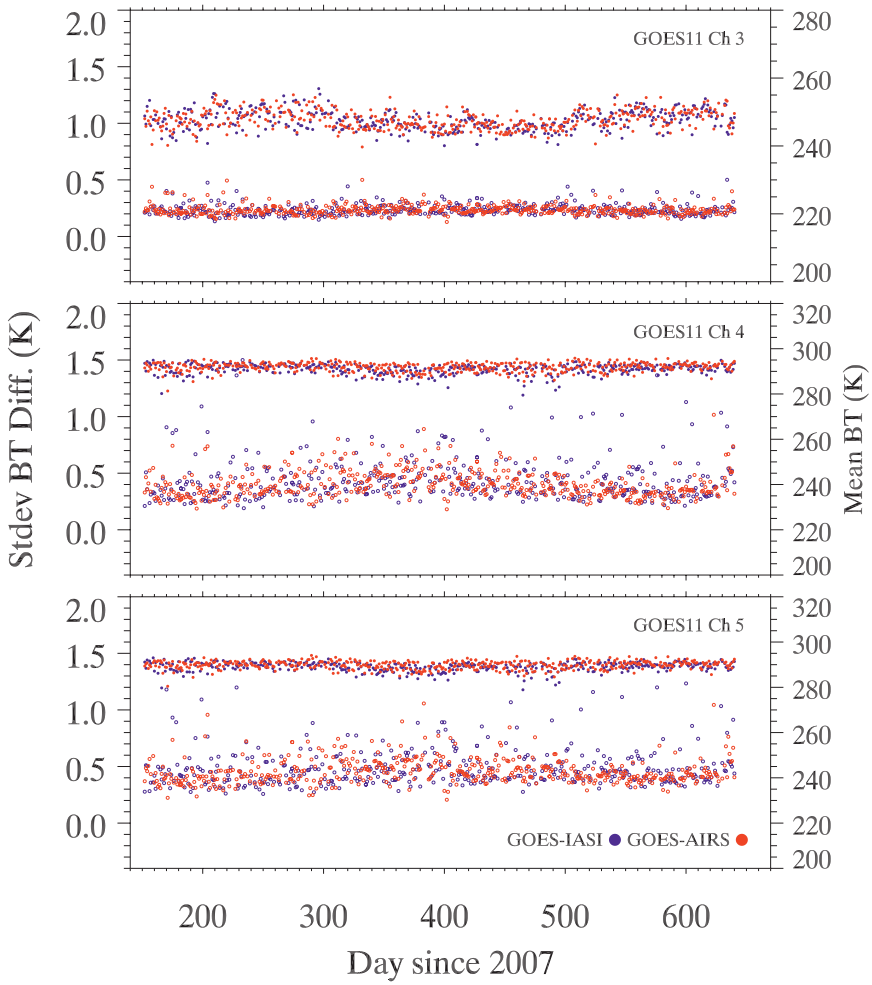

FIG. 9. As in Fig. 8, but for the *GOES-11* imager.

and then used the double differences between AIRS – RTGSST and IASI – RTGSST to investigate the AIRS and IASI radiance difference at 2616 cm^{-1}. This study demonstrates that the relatively stable GOES imager can be used as a transfer radiometer to indirectly compare two polar-orbiting sensors. However, in order to fully cancel the calibration bias of the transfer radiometer, the following conditions must be met. First, the transfer radiometer must be stable during the time period when two polar-orbiting satellites pass overhead. Second, coincident observations of two polar-orbiting instruments with the transfer radiometer are expected to be sampled in similar atmospheric conditions, which can avoid the calibration bias related to a specific atmospheric environment. The GOES mean BTs for AIRS–GOES and IASI–GOES collocated observations in Figs. 8 and 9 have similar values, and their time series remain constant during the study period, suggesting that the GOES–IASI and GOES–AIRS collocations are sampled in the same environmental conditions. The advantages of using geostationary imagers as transfer radiometers include 1) a large number of coincident collocations, 2) various spectral coverage patterns, 3) the capability of making comparisons in the tropical regions, and 4) cross validation by switching different geostationary imagers. We believe that the double-difference method proposed in this study allows for checking the AIRS and IASI calibration accuracy and stability over a long period of time.

For the AIRS and IASI radiance difference, Strow et al. (2008) used the double-difference method to compare AIRS and IASI at the finest scale by choosing radiative transfer calculations as a transfer target. Tobin et al. (2008) directly compared AIRS and IASI at the finest spectral scale based on the SNO observations. They both found that AIRS and IASI agree on the order of 0.1 K, while AIRS is slightly warmer than IASI. Aumann and Pagano (2008) chose RTGSST as a transfer target.

The double-difference statistics between AIRS and the RTGSST and IASI and the RTGSST also reveal a ~0.02 K difference, and indicate that AIRS is slightly warmer than IASI. Our analysis is consistent with their findings, though it is confined at the spectral regions covered by the GOES imagers.

4. Conclusions

Quantifying the radiometric difference and creating a calibration link between AIRS and IASI are crucial for creating fundamental climate data records and establishing the space-based calibration standard. This study proposes a method of comparing AIRS and IASI in the tropical regions using the GOES imagers as transfer radiometers. Specifically, the AIRS and IASI radiances are convolved with the GOES imager SRFs and then compared with the geostationary imager radiance measurements with common spatial and temporal collocation criteria. The double differences between the AIRS and IASI radiance biases relative to the GOES imagers are used to quantify the radiometric difference of the AIRS and IASI radiance measurements in terms of BT. The results indicate that the calculated double differences are not affected by the GOES imager calibration bias. This study demonstrates that stable geostationary instruments can be used as transfer radiometers to intercompare polar-orbiting hyperspectral instruments on different satellite platforms for warm scenes in tropical regions, which complements the direct comparison of IASI and AIRS using the simultaneous nadir overpass technique.

It is not possible, from this study, to address the absolute calibration accuracy for both the AIRS and IASI instruments by means of intersatellite comparison results. We thus focus on analyzing the relative bias between IASI and AIRS within the GOES imager spectral coverage during a 16-month time period. The results indicate that, at the 95% confidence level, the mean values of the IASI–AIRS brightness temperature differences are -0.0641 ± 0.0074 K, -0.0432 ± 0.0114 K, and -0.0095 ± 0.0151 K for the *GOES-11* 6.7-, 10.7-, and 12.0-μm channels, and -0.0490 ± 0.0100 K, -0.0419 ± 0.0224 K, and -0.0884 ± 0.0160 K for the *GOES-12* 6.5-, 10.7-, and 13.3-μm channels for typical warm scenes. While the results from the *GOES-12* 6.5-μm channel should be viewed with caution because of the spectral gap filling; they generally suggest that the radiance differences between AIRS and IASI within the GOES imager channels are less than 0.1 K while AIRS is slightly warmer than IASI.

As a final note, we point out that, due to the huge volume of AIRS, IASI, and geostationary imager data, this study is only limited to the GOES imagers. Second, the approach used in this study cannot be performed at the finest spectral scale, but instead is limited to the spectral coverage of transfer radiometers. Finally, the diurnal variation of the GOES imager calibration further confines the comparison to the longwave IR spectral regions. In the future, with the GOES-R Advance Baseline Imager, which has more spectral coverage and stable calibration, and the progress of the GSICS program, this method can be further extended to link the AIRS, IASI, and the Cross-track Infrared Sounder (CrIS) toward generating fundamental climate data records.

Acknowledgments. The authors thank Drs. Yong Han, Quanhau Liu, Cheng-Zhi Zou, and Robert Iacovazzi for their critical review and judicious comments, and the GSICS community for their advice and collaboration. Thanks are extended to Dr. Denis Blumstein of CNES for his help with IASI calibration issues, and Dr. Yong Chen of CSU for providing the IASI and AIRS spectra computed from CRTM. This study is partially funded by the IPO/IGS and STAR Cal/Val funds. We also appreciate the constructive comments by three anonymous reviewers. The manuscript contents are solely the opinions of the authors and do not constitute a statement of policy, decision, or position on behalf of NOAA or the U.S. government.

REFERENCES

Aumann, H. H., and T. S. Pagano, 2008: Using AIRS and IASI data to evaluate absolute radiometric accuracy and stability for climate applications. *Atmospheric and Environmental Remote Sensing Data Processing and Utilization IV: Readiness for GEOSS II,* M. D. Goldberg et al., Eds., International Society for Optical Engineering (SPIE Proceedings, Vol. 7085), doi:10.1117/12.795225.

Bevington, P. R., and D. K. Robinson, 2003: *Data Reduction and Error Analysis for the Physical Sciences*. 3rd ed. McGraw-Hill, 320 pp.

Blumstein, D., and Coauthors, 2004: IASI instrument: Technical overview and measured performances. *Infrared Spaceborne Remote Sensing XII,* M. Strojnik, Ed., International Society for Optical Engineering (SPIE Proceedings, Vol. 5543), 196–207.

——, B. Tournier, F. R. Cayla, T. Phulpin, R. Fjortoft, C. Buil, and G. Ponce, 2007: In-flight performance of the infrared atmospheric sounding interferometer (IASI) on METOP-A. *Atmospheric and Environmental Remote Sensing Data Processing and Utilization III: Readiness for GEOSS,* M. D. Goldberg et al., Eds., International Society for Optical Engineering (SPIE Proceedings, Vol. 6684), doi:10.1117/12.734162.

Boeing, 2006: GOES-N data user book. NASA GSFC Contract NAS5-98069, 220 pp.

Cao, C., M. Goldberg, and L. Wang, 2009: Spectral bias estimation of historical HIRS using IASI observations for improved fundamental climate data records. *J. Atmos. Oceanic Technol.,* **26,** 1378–1387.

Chahine, M. T., and Coauthors, 2006: Improving weather forecasting and providing new data on greenhouse gases. *Bull. Amer. Meteor. Soc.,* **87,** 911–926.

Goody, R., and R. Haskins, 1998: Calibration of radiances from space. *J. Climate,* **11,** 754–758.

Gunshor, M. M., T. J. Schmit, W. P. Menzel, and D. C. Tobin, 2009: Intercalibration of broadband geostationary imagers using AIRS. *J. Atmos. Oceanic Technol.,* **26,** 746–758.

Johnson, R. X., and M. P. Weinreb, 1996: GOES-8 imager midnight effects and slope correction in GOES-8 and beyond. *GOES-8 and Beyond,* E. R. Washwell, Ed., International Society for Optical Engineering (SPIE Proceedings, Vol. 2812), **2812,** 596–607.

Klaes, K. D., and Coauthors, 2007: An introduction to the EUMETSAT Polar System. *Bull. Amer. Meteor. Soc.,* **88,** 1085–1096.

Santer, B. D., T. M. L. Wigley, J. S. Boyle, D. J. Gaffen, J. J. Hnilo, D. Nychka, D. E. Parker, and K. E. Taylor, 2000: Statistical significance of trends and trend differences in layer-average atmospheric temperature time series. *J. Geophys. Res.,* **105,** 7337–7356.

Schmit, T. J., E. M. Prins, A. J. Schreiner, and J. J. Gurka, 2001: Introducing the GOES-M imager. *Natl. Wea. Dig.,* **25** (3–4), 28–37.

Strow, L., S. Hannon, D. Tobin, and H. Revercomb, 2008: Intercalibration of the AIRS and IASI operational infrared sensors. *Proc. 17th Annual Conf. on Characterization and Radiometric Calibration for Remote Sensing (CALCON),* Logan, UT, Utah State University Research Foundation, CD-ROM.

Tahara, Y., and K. Kato, 2008: New spectral compensation method for intercalibration with high spectral resolution sounder. Japan Meteorological Agency Meteorological Satellite Center Tech. Note 52, 37 pp. [Available online at http://mscweb.kishou.go.jp/monitoring/gsics/ir/techinfo.htm.]

Tobin, D. C., H. E. Revercomb, C. C. Moeller, and T. S. Pagano, 2006: Use of atmospheric infrared sounder high-spectral resolution spectra to assess the calibration of Moderate resolution Imaging Spectroradiometer on EOS Aqua. *J. Geophys. Res.,* **111,** D09S05, doi:10.1029/2005JD006095.

——, ——, F. Nagle, and R. Holz, 2008: Evaluation of IASI and AIRS spectral radiances using simultaneous nadir overpasses. *Proc. 16th Int. TOVS Study Conf.,* Angra dos Reis, Brazil, Int. TOVS Working Group. [Available online at http://cimss.ssec.wisc.edu/itwg/itsc/itsc16/posters/B07_dave_tobin.pdf.]

Wang, L., and C. Cao, 2008: On-orbit calibration assessment of AVHRR longwave channels on MetOp-A using IASI. *IEEE Trans. Geosci. Remote Sens.,* **46,** 4005–4013.

——, ——, and P. Ciren, 2007: Assessing *NOAA-16* HIRS radiance accuracy using simultaneous nadir overpass observations from AIRS. *J. Atmos. Oceanic Technol.,* **24,** 1546–1561.

——, ——, and M. D. Goldberg, 2009: Intercalibration of *GOES-11* and *GOES-12* water vapor channels with MetOp/IASI hyperspectral measurements. *J. Atmos. Oceanic Technol.,* **26,** 1843–1855.

Wu, A., X. Xiong, and C. Cao, 2008: *Terra* and *Aqua* MODIS intercomparison of three reflective solar bands using AVHRR onboard the NOAA-KLM satellites. *Int. J. Remote Sens.,* **29,** 1997–2010.

Wu, X., and M. Goldberg, 2007: Global space-based inter-calibration system (GSICS): A status report. *Atmospheric and Environmental Remote Sensing Data Processing and Utilization III: Readiness for GEOSS,* M. D. Goldberg et al., Eds., International Society for Optical Engineering (SPIE Proceedings, Vol. 6684), doi:10.1117/12.734127.